



Title	Red-emission over a wide range of wavelengths at various temperatures from tetragonal BaCN <sub>2</sub> :Eu <sup>2+</sup>
Author(s)	Masubuchi, Yuji; Nishitani, Sayaka; Hosono, Akira; Kitagawa, Yuuki; Ueda, Jumpei; Tanabe, Setsuhisa; Yamane, Hisanori; Higuchi, Mikio; Kikkawa, Shinichi
Citation	Journal of materials chemistry C, 6(24), 6370-6377 <a href="https://doi.org/10.1039/c8tc01289j">https://doi.org/10.1039/c8tc01289j</a>
Issue Date	2018-06-28
Doc URL	<a href="http://hdl.handle.net/2115/74809">http://hdl.handle.net/2115/74809</a>
Type	article (author version)
File Information	JMaterChemC2018-6370-6377.pdf



[Instructions for use](#)



Received 00th January  
20xx,

Accepted 00th January 20xx

DOI: 10.1039/x0xx00000x

[www.rsc.org/](http://www.rsc.org/)

## Red-emission over a wide range of wavelength at various temperatures from tetragonal BaCN<sub>2</sub>:Eu<sup>2+</sup>

Yuji Masubuchi<sup>a\*</sup>, Sayaka Nishitani<sup>b</sup>, Akira Hosono<sup>b</sup>, Yuuki Kitagawa<sup>c</sup>, Jumpei Ueda<sup>c</sup>, Setsuhisa Tanabe<sup>c</sup>, Hisanori Yamane<sup>d</sup>, Mikio Higuchi<sup>a</sup>, Shinichi Kikkawa<sup>a</sup>

A new polymorph of BaCN<sub>2</sub> was obtained via a simple nitridation reaction of BaCO<sub>3</sub> under an NH<sub>3</sub> flow at 900 °C. The product was analyzed by single crystal X-ray diffraction and infrared spectroscopy, and found to have a tetragonal *I4/mcm* crystal structure (space group no. 140) with  $a = 0.60249(4)$  nm and  $c = 0.71924(5)$  nm. In this structure, each Ba<sup>2+</sup> cation is situated in the square antiprism of N atoms of NCN<sup>2-</sup> anionic groups. Eu<sup>2+</sup> doped BaCN<sub>2</sub> can be excited by irradiation of blue and green light (from 400 to 550 nm), and generates an intense red emission peak at 660 nm with a quantum efficiency of 42% in response to 465 nm excitation at room temperature. The peak emission wavelength varies over an extremely wide range with temperature, from 640 nm at 500 K to 680 nm at 80 K, and this red-shift with decreasing temperature is attributed to a unit cell shrinkage that results in significant crystal field splitting of the 5d energy levels of the Eu<sup>2+</sup> ions.

### Introduction

Many inorganic materials, including oxides, nitrides, sulfides, and chalcogenides, have been developed as host materials for phosphors<sup>1-3</sup>. Divalent Eu-doped nitride phosphors are especially widely studied because of their superior thermal and chemical stabilities of their optical properties. High performance nitride phosphors are already used for commercial LED applications<sup>4,5</sup>. The emission spectra of Eu<sup>2+</sup>-doped phosphors are typically characterized by the parity-allowed transition from the 4f<sup>7</sup> to the 4f<sup>6</sup>5d<sup>1</sup> state. The energy of the 4f<sup>6</sup>5d<sup>1</sup> excited state is closely correlated with various structural parameters, such as covalency, bond length, and coordination number. These factors determine the crystal field strength and the nephelauxetic effect that in turn modify the emission properties. Therefore the luminescence characteristics obtained from Eu<sup>2+</sup> doping can be tailored by choosing a suitable host material.

Metal cyanamides and carbodiimides are interesting inorganic materials that exhibit a nitrogen-related pseudo-oxide chemistry, since NCN<sup>2-</sup> anionic groups can replace O<sup>2-</sup> anions. The triatomic anionic groups in these compounds can have varying numbers of

neighboring metal cations and thus form a characteristic host lattice depending on the cation. Many transition metal cyanamides have been prepared via solution process. As an example, CuCN<sub>2</sub>, ZnCN<sub>2</sub> and CdCN<sub>2</sub> can be obtained from the reaction of the associated metal chlorides and cyanamide in aqueous media<sup>6-8</sup>. Solid-state metathesis has also resulted in the formation of MnCN<sub>2</sub> from MnCl<sub>2</sub> and ZnCN<sub>2</sub><sup>9</sup>, while SrCN<sub>2</sub> was synthesized via a flux route based on a combination of a strontium halide, alkaline cyanide, and alkaline azide precursors<sup>10</sup>. Calcium carbide has also been used as the starting material to form CaCN<sub>2</sub> under a pressurized N<sub>2</sub> atmosphere<sup>11</sup>, and the high temperature nitridation reactions of CaCO<sub>3</sub> and SrCO<sub>3</sub> under an ammonia flow have also been applied to synthesize the respective cyanamides<sup>12,13</sup>. The rhombohedral structure (*R*-3c) of BaCN<sub>2</sub> with  $a = 1.5282(2)$  nm and  $c = 0.7013(2)$  nm has only been reported for a cyanamide prepared from the reaction of Ba<sub>3</sub>N<sub>2</sub> and melamine under an Ar flow at temperatures between 740 °C and 850 °C<sup>14</sup>. In this structure, six N atoms of NCN<sup>2-</sup> coordinate to each Ba<sup>2+</sup> cation, forming a distorted octahedron. In addition, only formation of BaCN<sub>2</sub> has been reported in the reaction of BaCO<sub>3</sub> with hydrogen cyanide or the nitridation reaction of BaCO<sub>3</sub><sup>12,15</sup>.

Alkaline earth cyanamides and related compounds such as metal cyanate (MOCN) and thiocyanate (MSCN) have been applied as host materials for Eu<sup>2+</sup> doping. A blue emission peak at 457 nm is generated by Eu<sup>2+</sup>-doped Sr(OCN)<sub>2</sub>, while Eu<sup>2+</sup>-doped Sr(SCN)<sub>2</sub> produces a green emission at 508 nm in response to excitation at 420 nm<sup>16,17</sup>. A longer emission wavelength of 610 nm (corresponding to orange color) has been reported for Eu<sup>2+</sup>-doped α-SrCN<sub>2</sub><sup>13</sup>. However, these characteristic emissions are only evident at low temperatures and are completely quenched at room temperature. Their thermal quenching temperatures ( $T_{1/2}$ ) at which the luminescence intensities are reduced by 50% are 65 K, 157 K

<sup>a</sup> Faculty of Engineering, Hokkaido University, N13 W8, Kita-ku, Sapporo 060-8628, Japan. E-mail: yuji-mas@eng.hokudai.ac.jp

<sup>b</sup> Graduate School of Chemical Science and Engineering, Hokkaido University, N13 W8, Kita-ku, Sapporo 060-8628, Japan

<sup>c</sup> Graduate School of Human and Environmental Studies, Kyoto University, Yohida-nihonmatsu-cho, Sakyo-ku, Kyoto 606-8501, Japan

<sup>d</sup> Institute of Multidisciplinary Research for Advanced Materials, Tohoku University, 2-1-1 Katahira, Aoba-ku, Sendai 980-8577, Japan

† Electronic Supplementary Information (SEI) available: Crystallographic Data (CSD 434273) in CIF format, powder XRD, lattice parameters. See DOI: 10.1039/x0xx00000x

and 90 K for Eu<sup>2+</sup>-doped Sr(OCN)<sub>2</sub>, Sr(SCN)<sub>2</sub> and α-SrCN<sub>2</sub>, respectively. However, a room temperature orange emission at 603 nm has been reported for the Eu<sup>2+</sup>-doped α-SrCN<sub>2</sub> obtained from the reaction of SrI<sub>2</sub>, EuI<sub>2</sub>, CsN<sub>3</sub> and CsCN in Ta ampules<sup>10</sup>. This emission at room temperature has been attributed to the reduced defect concentration caused by direct doping with Eu<sup>2+</sup>I<sub>2</sub>. Ba(SCN)<sub>2</sub> was also studied as a host material with regard to doping with Eu<sup>2+</sup><sup>18</sup>. Ba<sup>2+</sup> was coordinated with eight SCN<sup>-</sup> anionic groups to form distorted square antiprism polyhedra. This material was found to generate an intense bright green emission peak at 511 nm at low temperature that was completely quenched at room temperature, with a  $T_{1/2}$  of 181 K.

In this paper, we present the crystal structure of a new polymorph of barium carbodiimide (BaCN<sub>2</sub>) prepared by a simple nitridation reaction of BaCO<sub>3</sub>. This polymorph crystallized in a tetragonal lattice with square antiprism coordination around the Ba<sup>2+</sup> ions, and was studied as a novel host material for Eu<sup>2+</sup> ions. Eu<sup>2+</sup>-doped BaCN<sub>2</sub> was found to produce a red emission over a wide range of wavelengths depending on temperature, and these emission characteristics were investigated in relation to the crystal structure.

## Experimental

### Synthesis procedures

The new polymorph of BaCN<sub>2</sub> was prepared via the heating of BaCO<sub>3</sub> (99.9% purity, Wako Pure Chemicals Co.) on an aluminum boat under a 50 mL min<sup>-1</sup> of NH<sub>3</sub> flow at 900 °C for 15 h. Eu<sup>2+</sup>-doped BaCN<sub>2</sub> was also prepared from a mixture of BaCO<sub>3</sub> and Eu acetylacetone hydrate (Eu(acac)<sub>3</sub>*n*H<sub>2</sub>O where *n* = 1.8, 99.9%, Aldrich). These two powders were mixed at a Ba:Eu ratio of 1-x:x (*x* = 0.002-0.05) in ethanol and subsequently nitrided under the same conditions as that for non-doped BaCN<sub>2</sub>. The nitrided products were found to be air-sensitive, so the characterization described below was performed under either a dry N<sub>2</sub> atmosphere or vacuum.

### Structural analysis

Crystalline phases were characterized using powder X-ray diffraction (XRD: Rigaku, Ultima IV) with Cu Kα radiation. The products were contained in an air-tight sample holder. acum. Single-crystal XRD data were collected by the ω/φTemperature dependence of powder XRD pattern was also measured using XRD (Rigaku, Ultima III) equipped with low temperature chamber unit (Anton Paar, TTK 450) over the range of 138 – 500 K, under vscans method with a diffractometer, employing Mo Kα radiation (Bruker, D8 QUEST). Data collection and unit-cell refinement were performed with the APEX2 software package<sup>19</sup>. Absorption corrections were applied using the SADABS multiscan procedure<sup>20</sup>, the structural parameters of the crystal were refined with the SHELXL-2014 program<sup>21</sup> and the crystal structures were drawn using the VESTA program<sup>22</sup>. The temperature dependence of the lattice parameters was also determined for a BaCN<sub>2</sub> crystal over the range of 90 K to 290 K with the diffractometer equipped with a cryostream (Oxford Cryosystem, Cobura). The powder XRD pattern of

BaCN<sub>2</sub> was calculated using the Rietveld program RIETAN-FP<sup>23</sup> based on the refined structural parameters.

### Chemical composition

The Ba content in the specimens was determined by inductively coupled plasma-atomic emission spectroscopy (ICP-AES: Shimadzu, ICPE-9000) after dissolving a 10 mg sample in diluted nitric acid. The C, H, and N levels were assessed via C/H/N analysis (Exeter Analytical, Inc., CE440) while the O content was also measured using a combustion analyzer (Horiba, EMGA-620).

### XANES

Eu L<sub>III</sub>-edge X-ray absorption near edge structure (XANES) data were acquired in the transmission mode at the BL-9C beam line of the Photon Factory at the High Energy Accelerator Research Organization (KEK), Tsukuba, Japan, with the storage ring operating at 2.5 GeV. A small amount of the sample powder was mixed with BN powder and then pressed into a pellet for the measurements. EuCl<sub>2</sub> and Eu<sub>2</sub>O<sub>3</sub> were used as references.

### FT-IR spectroscopy

Fourier transform infrared spectroscopy (FT-IR) was performed with an FT-IR/4700 spectrometer (Jasco). Test specimens were prepared by sandwiching BaCN<sub>2</sub> powder between KBr plates and pressing the sample into a pellet under a dry nitrogen atmosphere.

### Optical measurements

Photoluminescence spectra were acquired at room temperature with a fluorescence spectrometer (Jasco, FP-6500) equipped with a 150 W Xe lamp as an excitation source. The temperature dependence of luminescence was assessed over the range of 80 – 500 K using a multichannel spectrometer (Ocean Optics, QE65 Pro) with 460 nm excitation by an LED in conjunction with a band-pass filter. During the measurement, the phosphor powder was heated from 80 K to 500 K and then cooled to 80 K in 5 K intervals at a heating/cooling rate of 10 K/min, under vacuum.

The total radiant flux spectra of the pump-LED source and sample luminescence under direct- and indirect- excitation of the sample were measured with an integrating sphere (Labsphere, LMS-100). The measured spectra were calibrated with a standard halogen lamp (Labsphere, CLS-600) to obtain the precise spectral power distributions, from which photon emission rate of the pump-LED under direct- and indirect-excitation,  $\Phi_{ex\_direct}(\lambda)$  and  $\Phi_{ex\_indirect}(\lambda)$  and that of sample luminescence under direct- and indirect excitation,  $\Phi_{lumin\_direct}(\lambda)$  and  $\Phi_{lumin\_indirect}(\lambda)$  can be calculated. Quantum efficiency (QE) values were calculated using the following equation:

$$QE = \frac{\int \{ \Phi_{lumin\_direct}(\lambda) - \Phi_{lumin\_indirect}(\lambda) \} d\lambda}{\int \{ \Phi_{ex\_indirect}(\lambda) - \Phi_{ex\_direct}(\lambda) \} d\lambda} \quad (1)$$

The luminescence spectra used to determine the QE were recorded using the multichannel spectrometer.

The fluorescence decay curves monitoring 650 nm luminescence were measured with Quantaurus-Tau (Hamamatsu Photonics, C11367-01) under 365 nm picosecond LED excitation at different temperatures from 90 to 450 K. The temperature of the sample was controlled by a cryostat (Japan High Tech, 10035L). The obtained fluorescence decay curve was fitted after baseline subtraction using a single-exponential function,

$$I(T) = I_0 \times \exp(-t/\tau) \quad (2)$$

$I_0$  is initial intensity and  $\tau$  is lifetime.

## Results and discussion

### Crystal structure of the BaCN<sub>2</sub> polymorph

The powder XRD pattern of the product is shown in Fig. S1 (Electronic Supplementary Information), where it is compared with the pattern calculated for rhombohedral (*R*-3c) BaCN<sub>2</sub> reported by W. Schnick<sup>14</sup>. From these patterns, it is evident that rhombohedral BaCN<sub>2</sub> phase does not appear even as an impurity phase. The Ba concentration in the product was found to be 77.3(9) wt%, while C, H, and N contents were 6.83(2), <0.30 and 15.42(5) wt%, respectively. The H and O levels were below the detection limits of the C/H/N and the combustion analyses, respectively. From these data, the chemical formula for the compound was determined to be Ba<sub>1</sub>C<sub>1.01(1)</sub>N<sub>1.96(2)</sub>, which is consistent with BaCN<sub>2</sub>. Thus, the product obtained by the nitridation of BaCO<sub>3</sub> is a new polymorph of BaCN<sub>2</sub>.

The crystal structure of the BaCN<sub>2</sub> polymorph was analyzed by single crystal XRD. The structure was refined to give the tetragonal space group *I*4/*mcm* (no. 140) with  $a = 0.60249(4)$  nm and  $c = 0.71924(5)$  nm, and  $Z = 4$  (Table 1). The atomic coordinates and anisotropic displacement parameters are given in Table 2. This structure is an isotype of that of the alkaline cyanates, AOCN ( $A = K$ , Rb, or Cs)<sup>24,25</sup>, in which each Ba<sup>2+</sup> ion is coordinated with eight N atoms belonging to NCN<sup>2-</sup> groups (Fig. 1), and in the regular square antiprism of N. The NCN<sup>2-</sup> anion is in the square prism of Ba atoms (Fig. 1(c)). The Ba-centered square antiprism polyhedra are connected via face sharing along the *c*-axis and edge-sharing in the *ab*-plane. Along the *c*-axis, Ba<sup>2+</sup> and NCN<sup>2-</sup> layers are stacked on one another along the *c*-axis to form a CsCl-type arrangement of both ions in conjunction with an ordered arrangement of the NCN<sup>2-</sup> groups. The C–N bond length is 0.1233(7) nm (Table 3), which corresponds to values reported for C–N double bonds in metal cyanamides<sup>14</sup>. This value is respectively longer and shorter than the C–N triple and single bonds in PbCN<sub>2</sub> (0.1156 nm for triple and 0.1297 nm for single)<sup>26</sup>. The Ba–N bond length in this new polymorph is 0.2928(5) nm, which is longer than the values reported for rhombohedral BaCN<sub>2</sub> having the octahedral coordinated Ba<sup>2+</sup> cations (0.2773 – 0.2867 nm)<sup>14</sup>. The face-sharing Ba<sup>2+</sup> polyhedra along the *c*-axis result in a Ba–Ba distance of 0.35962(3) nm, whereas the distance in the *ab*-

plane that is 0.42602(2) nm and thus similar to that in rhombohedral BaCN<sub>2</sub>.

Table 1 Crystal data and refinement result for BaCN<sub>2</sub> obtained by the nitridation reaction of BaCO<sub>3</sub>

<i>Chemical formula</i>	BaCN <sub>2</sub>
<i>Formula weight, M<sub>r</sub> (g mol<sup>-1</sup>)</i>	177.37
<i>Crystal form, color</i>	Granule, Translucent colorless
<i>Crystal size, mm<sup>3</sup></i>	0.064×0.052×0.036
<i>Radiation wavelength, λ (nm)</i>	0.071073
<i>Temperature, T (K)</i>	302
<i>Crystal system</i>	Tetragonal
<i>Space group</i>	<i>I</i> 4/ <i>mcm</i> (No. 140)
<i>Unit-cell dimensions, a (nm)</i>	0.60249(4)
<i>c (nm)</i>	0.71924(5)
<i>Unit-cell volume, V (nm<sup>3</sup>)</i>	0.26108(4)
<i>Z</i>	4
<i>Calculated density, D<sub>cal</sub> (Mg m<sup>-3</sup>)</i>	4.512
<i>Absorption coefficient, μ (mm<sup>-1</sup>)</i>	14.862
<i>Absorption correction</i>	MULTI-SCAN (SADABS) <sup>20</sup>
<i>Limiting Indices</i>	-7 ≤ <i>h</i> ≤ 7 -7 ≤ <i>k</i> ≤ 7 -9 ≤ <i>l</i> ≤ 9
<i>Number of reflections</i>	92
<i>Weight parameters, a, b</i>	0.0156, 4.0817
<i>Goodness-of-fit on F<sup>2</sup>, S</i>	1.392
<i>R</i> 1, <i>wR</i> 2( <i>I</i> > 2σ( <i>I</i> ))	0.0206, 0.0441
<i>R</i> 1, <i>wR</i> 2(all data)	0.0246, 0.0454

$R1 = \sum |F_o| - |F_c| | / \sum |F_o|$ .  $wR2 = [\sum w(F_o^2 - F_c^2)^2 / \sum (wF_o^2)^2]^{1/2}$ ,  $w = 1 / [(\sigma^2(F_o^2) + (aP)^2 + bP)]$ , where  $F_o$  is the observed structure factor,  $F_c$  is the calculated structure factor,  $\sigma$  is the standard derivation of  $F_c^2$ , and  $P = (F_o^2 + 2F_c^2)/3$ .  $S = [\sum w(F_o^2 - F_c^2)^2 / (n-p)]^{1/2}$ , where  $n$  is the number of reflections and  $p$  is the total number of parameters refined.

Table 2 Atomic coordinates and anisotropic displacement parameters for BaCN<sub>2</sub>

Atom	Site	Occ.	x	y	z
Ba	4a	1	0	0	0.25
C	4d	1	0.5	0	0
N	8h	1	0.3533(11)	0.1447(11)	0

Atom	Site	$U_{11} = U_{22}$	$U_{33}$	$U_{12}$	$U_{23}$	$= U_{13}$
Ba	4a	0.0106(3)	0.0118(4)	0	0	
C	4d	0.008(3)	0.009(5)	0.003(9)	0	
N	8h	0.008(2)	0.015(4)	-0.001(3)	0	

$U_{ij} / \times 10^{-2} \text{ nm}^2 (= \text{\AA}^2)$

Table 3 Selected bond lengths (nm) for tetragonal BaCN<sub>2</sub>

C–N	×2	0.1233(7)
Ba–N	×8	0.2928(5)
Ba–Ba	×2	0.35962(3)

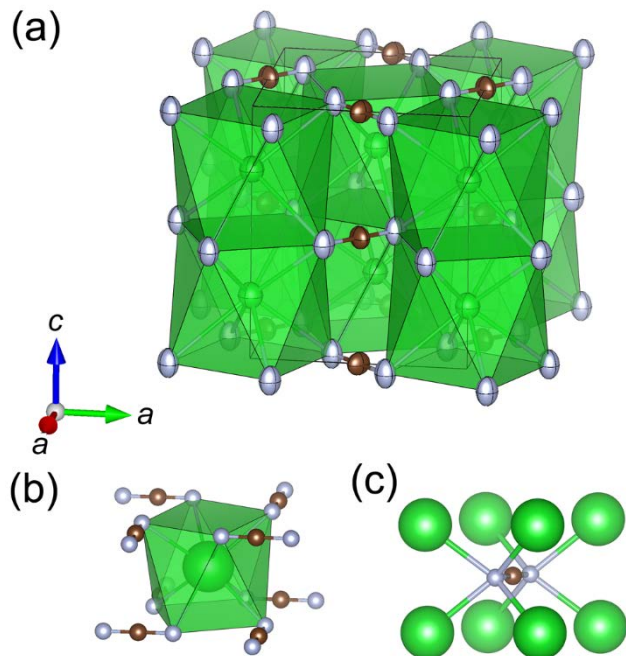
*x4*      0.42602(2)

Figure 1 (a) The crystal structure of tetragonal  $\text{BaCN}_2$  (anisotropic ellipsoids drawn at the 99% probability level). Coordination around (b) Ba and (c) NCN atoms (green, brown, and grey spheres correspond to Ba, C and N atoms, respectively).

The FT-IR spectrum of this compound exhibits an asymmetric stretch peak ( $\nu_{as}$ ) at  $1960 \text{ cm}^{-1}$  and deformation vibration peaks ( $\delta$ ) at  $670$  and  $680 \text{ cm}^{-1}$  (Fig. 2). These peak positions are in good agreement with those generated by both rhombohedral  $\text{BaCN}_2$  and  $\alpha\text{-SrCN}_2$ , each of which are metal carbodiimides having two symmetric  $\text{N}=\text{C}=\text{N}$  double bonds<sup>10,14</sup>. The tetragonal  $\text{BaCN}_2$  obtained in this work is therefore believed to contain carbodiimide anions ( $[\text{N}=\text{C}=\text{N}]^{2-}$ ). To confirm the tetragonal structure, a powder XRD pattern was calculated using the Rietveld program based on the structural parameters in Tables 1 and 2, and a comparison of the observed and the calculated powder XRD patterns is presented in Fig. 3. The experimental diffraction lines are in good agreement with the calculated pattern, although several additional weak reflections are also present in the former. The impurity phase associated with these reflections has not yet been identified but might consist of a metal cyanamide having both triple and single bonds between C and N, for which there is some evidence in the FT-IR spectrum (Fig. 2).

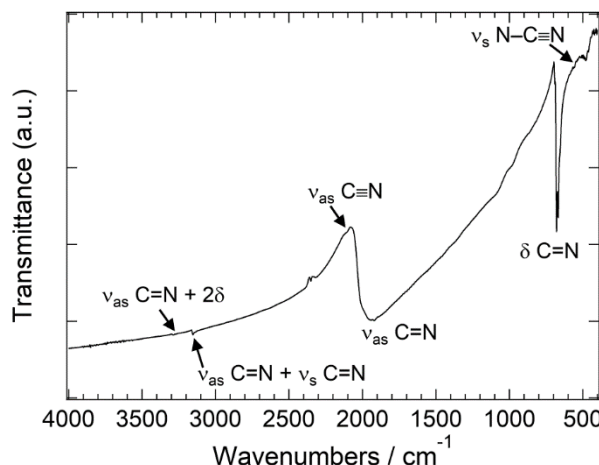


Figure 2 The FT-IR spectrum of the nitrided product. The symbols,  $\nu_{as}$ ,  $\nu_s$ , and  $\delta$  correspond to the absorptions for asymmetric stretch, symmetric stretch and deformation vibrations, respectively.

Thermogravimetric and differential thermal analyses (TG-DTA) for the tetragonal  $\text{BaCN}_2$  under a  $\text{N}_2$  flow was performed in our previous study and indicates an endothermic peak at approximately  $910 \text{ }^\circ\text{C}$  without a weight loss corresponding to the melting of  $\text{BaCN}_2$ <sup>27</sup>. A solidified product of the  $\text{BaCN}_2$  after annealing above the melting temperature contains the rhombohedral  $\text{BaCN}_2$  instead of the tetragonal phase. We did not find an additional signal in the DTA curve indicating the phase transition, however we believe the transition temperature was obscured by the large endothermic peak of the melting and the high temperature phase is the rhombohedral  $\text{BaCN}_2$ . The phase transition from the tetragonal to rhombohedral  $\text{BaCN}_2$  is irreversible because there is no trace of the tetragonal phase in the XRD pattern of the annealed product. Density of the tetragonal  $\text{BaCN}_2$  is  $4.512 \text{ g/cm}^3$  which is larger than that of the rhombohedral  $\text{BaCN}_2$  ( $3.738 \text{ g/cm}^3$ )<sup>14</sup>. Interestingly, low-temperature but high-symmetry phase ( $I4/mcm$ ) transformed to the high-temperature but low-symmetry ( $R-3c$ ) phase. The mechanism of the phase transition is still unknown, however this counterintuitive phase transition was also reported in  $\text{SrCN}_2$ , in which phase transition from hexagonal high-symmetry  $\beta$ -phase to orthorhombic low-symmetry  $\alpha$ -phase occurs around  $920 \text{ K}$  and the phase transition is irreversible upon cooling similar to the case of  $\text{BaCN}_2$ <sup>28</sup>.

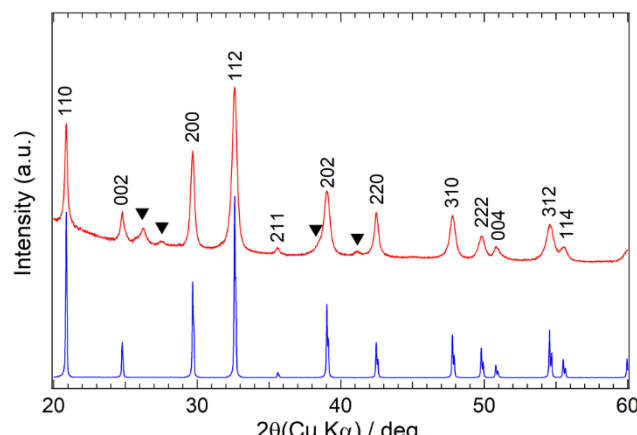


Figure 3 The powder XRD pattern of the nitrided product (red line) and the pattern calculated using the structural parameters in Tables 1 and 2 (blue line). Black triangles indicate diffraction lines attributed to an impurity phase.

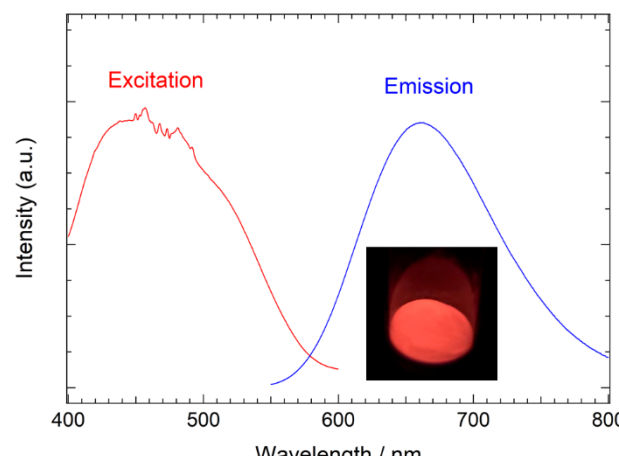


Figure 4 Emission and excitation spectra for the 1 at%  $\text{Eu}^{2+}$ -doped  $\text{BaCN}_2$ . The emission spectrum was acquired with excitation at 435 nm and the excitation spectrum was obtained based on emission at 660 nm. The inset shows the red emission of the product under UV light (365 nm) irradiation.

### Luminescence properties

$\text{Eu}^{2+}$ -doped tetragonal  $\text{BaCN}_2$  was obtained via the nitridation of a mixture of  $\text{BaCO}_3$  and  $\text{Eu}(\text{acac})_3 \cdot n\text{H}_2\text{O}$  under a flow of  $\text{NH}_3$ . The lattice parameters of the tetragonal  $\text{BaCN}_2$  were found to decrease with increasing  $\text{Eu}^{2+}$  contents, eventually reaching constant values at 1 at%  $\text{Eu}^{2+}$ , as shown in Fig. S2. This result indicates that the  $\text{Eu}^{2+}$  ions were incorporated into the tetragonal  $\text{BaCN}_2$  lattice. The photoluminescence properties of the 1 at% of  $\text{Eu}^{2+}$ -doped tetragonal  $\text{BaCN}_2$  were assessed, and a single broad red emission peak at 660 nm ( $15152 \text{ cm}^{-1}$ ) was observed in response to excitation at 435 nm. The full width at half maximum of this peak was 120 nm ( $2777 \text{ cm}^{-1}$ ), as can be seen in Fig. 4. An excitation band ranging from 400 to 550 nm with two maxima at 435 nm ( $22989 \text{ cm}^{-1}$ ) and 500 nm ( $20000 \text{ cm}^{-1}$ ) was observed upon monitoring the emission at 660 nm. The presence of  $\text{Eu}^{2+}$  in the phosphor was supported by an absorption peak at 6972 eV in the  $\text{Eu L}_{\text{III}}$ -edge XANES data, which is good agreement with the absorption energy for  $\text{EuCl}_2$ . Both the excitation and emission of this compound are attributed to the transitions between the  $4f^7$  and  $4f^65d^1$  energy levels of the  $\text{Eu}^{2+}$  ions. The red emission could be excited by irradiation at approximately 450 nm, which is the most commonly used wavelength in LEDs. Varying the  $\text{Eu}^{2+}$  concentration did not change the emission peak position significantly, indicating that the  $\text{Eu}^{2+}$  ion underwent low fluctuations in the chemical environment with increasing the  $\text{Eu}^{2+}$  concentrations. The QE of the red emission with excitation at 465 nm was found to be 42% at room temperature.

The Luminescence of  $\text{Eu}^{2+}$  ions in a host material is influenced by structural parameters, including covalency, bond-length and coordination number, and the  $4f$ – $5d$  transition energy of phosphors doped with  $\text{Eu}^{2+}$  can be estimated by using an empirical equation<sup>29,30</sup>. The equation indicates that an increase in the coordination number and the size of the substituted cation will induce a blue-shift in the emission wavelength of a  $\text{Eu}^{2+}$ -doped phosphor. As noted, red emission at 660 nm was observed in the case of the  $\text{Eu}^{2+}$ -doped tetragonal  $\text{BaCN}_2$ . By comparing its crystal structure with that of  $\text{Ba}(\text{SCN})_2:\text{Eu}^{2+}$ , which emits green light at 511 nm, it is evident that the tetragonal  $\text{BaCN}_2$  had a shorter Ba–N bond length (0.2928(5) nm) compared to the Ba–N (and S) bonds in  $\text{Ba}(\text{SCN})_2$ , for which the average bond length is 0.3086 nm<sup>18</sup>. The  $\text{Ba}^{2+}$  ions in the  $\text{BaCN}_2$  were coordinated in a regular square antiprism ( $D_{4d}$  point symmetry) environment having identical Ba–N bond lengths, while  $\text{Ba}(\text{SCN})_2$  is based on distorted square antiprism coordination ( $C_2$  point symmetry) in association with a wide range of Ba–N and Ba–S bond lengths. The greater negative charge of the  $\text{NCN}^{2-}$  anions forming the symmetric environment in  $\text{BaCN}_2$  will tend to stabilize the  $d$  orbitals of the  $\text{Eu}^{2+}$  ions, in contrast to the distorted coordination of monovalent  $\text{SCN}^-$  anions. As a result, increased crystal field splitting is expected in the  $\text{BaCN}_2$  host material, leading to the red emission of the  $\text{Eu}^{2+}$ -doped  $\text{BaCN}_2$ , because of the reduced energy difference between the  $4f^7$  ground state and the  $4f^65d^1$  excited state. Conversely, this explanation does not support the shorter emission wavelength of  $\text{Eu}^{2+}$ -doped  $\text{SrCN}_2$ , in which each cation is coordinated with six  $\text{NCN}^{2-}$  anions in a distorted octahedral environment<sup>13,17</sup>. The empirical equation noted above is, of course, not applicable to all phosphors. As an example, the emission peak is shifted toward longer wavelengths upon changing the  $M$  site cation from  $\text{Ca} \rightarrow \text{Sr} \rightarrow \text{Ba}$  in  $M_2\text{Si}_5\text{N}_8:\text{Eu}^{2+}$  ( $\text{Ca}_2\text{Si}_5\text{N}_8$ : 610 nm,  $\text{Sr}_2\text{Si}_5\text{N}_8$ : 630 nm,  $\text{Ba}_2\text{Si}_5\text{N}_8$ : 640 nm)<sup>31</sup>. The equation does not take into account the effect of site symmetry on the emission peak shift, so the symmetric square antiprism coordination in  $\text{BaCN}_2$  might increase the crystal field splitting to a great extent than

distorted octahedral coordination, such that the energy position of the 5d excited state is reduced.

### Temperature dependence of luminescence

The effects of temperature on emission were examined between 80 K and 500 K. As shown in Fig. 5, the emission peak wavelength shifts from 680 nm at 80 K to 640 nm at 500 K, and the thermal quenching temperature ( $T_{1/2}$ ), at which the emission intensity is reduced by 50%, was approximately 400 K. Both emission intensity and peak wavelength were recovered upon again decreasing the temperature (Figs. 5(b) and 5(c)). This strong red emission at ambient temperature is in contrast to that of Eu<sup>2+</sup>-doped Ba(SCN)<sub>2</sub>, which is a green phosphor with a lower  $T_{1/2}$  of 181 K. Reduced thermal quenching is usually associated with a small Stokes shift. As an example, Eu<sup>2+</sup>-doped SrLiAl<sub>3</sub>N<sub>4</sub> shows narrow band red emission with minimal thermal quenching and has an estimated Stokes shift of 956 cm<sup>-1</sup><sup>32</sup>. Minimal thermal quenching is also observed for  $\alpha$ -Sialon:Eu<sup>2+</sup> and CaAlSiN<sub>3</sub>:Eu<sup>2+</sup> phosphors, which have Stokes shifts of 5011 cm<sup>-1</sup> and 2000 cm<sup>-1</sup>, respectively<sup>33,34</sup>. According to P. Dorenbos, the energy position of the lowest excited 4f<sup>6</sup>5d<sup>1</sup> state can be estimated at about 20% of the excitation maximum to be 17762 cm<sup>-1</sup><sup>35</sup>. It leads to a Stokes shift of about 2610 cm<sup>-1</sup>, which is comparable to that of the nitride phosphors having excellent thermal stability. A larger Stokes shift in a Eu<sup>2+</sup>-doped phosphor has been reported to occur in a more asymmetric activator site geometry, because of a significant reorganization of anions about the Eu<sup>2+</sup> emission center under photoexcitation<sup>36,37</sup>. In contrast, the presence of alkaline earth ions having larger ionic radii in the host lattice results in a smaller Stokes shift because of restricted structural relaxation around the activator in its excited state<sup>38</sup>. The Ba<sup>2+</sup> sites in the BaCN<sub>2</sub> are coordinated in symmetric environment, each of which has an identical activator-N bond length. So the smaller Stokes shift in the Eu<sup>2+</sup>-doped BaCN<sub>2</sub> is related with the symmetric geometry of Ba site and large bond length.

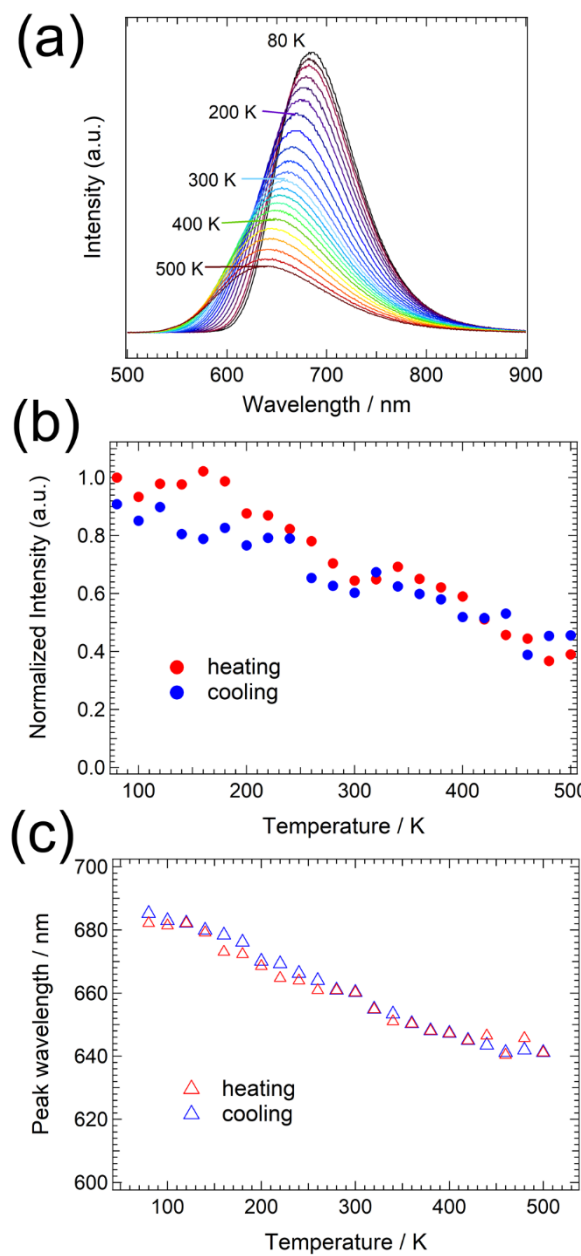


Figure 5 (a) Temperature dependence of the emission spectrum of the 1 at% Eu<sup>2+</sup>-doped tetragonal BaCN<sub>2</sub> with excitation at 460 nm. Temperature dependence of the (b) integrated intensity and (c) emission peak wavelength.

Thermally stable phosphors such as nitrides mentioned above do not exhibit significant changes in emission wavelength with increasing temperature (typically less than 1 nm on going from room temperature to 423 K and above), which is indicative of the high thermal stability of the chromatic behavior<sup>32-34</sup>. This thermal stability is caused by a rigid structure constructed from [SiN<sub>4</sub>] and/or [AlN<sub>4</sub>] tetrahedra. However, a large shift in the emission wavelength (from 680 nm at 80 K to 640 nm at 500 K) of the BaCN<sub>2</sub>:Eu<sup>2+</sup> is evident in Fig. 5(c). In the case of nitride phosphors, the emission wavelength is usually tailored by substitution between alkaline earth ions that modifies the environment around the activator ions, such as the crystal field strength, symmetry and polyhedron volume. As an example, a

blue shift in the emission spectrum is observed for  $\text{CaAlSiN}_4:\text{Eu}^{2+}$  upon substituting Sr for Ca.<sup>39</sup> The emission peak shifts from 650 nm for  $\text{CaAlSiN}_4:\text{Eu}^{2+}$  to 610 nm for  $\text{SrAlSiN}_4:\text{Eu}^{2+}$ , which has a 4% larger unit cell volume. In addition, a red shift of the emission peak of the  $\text{Sr}_2\text{Si}_5\text{N}_8:\text{Eu}^{2+}$  phosphor is achieved by replacing Sr with Ca, accompanied by a reduction in the unit cell volume<sup>40</sup>. To assess these effects in the present material, the temperature dependence of the lattice parameters of  $\text{BaCN}_2$  was examined between 90 K and 290 K. The normalized lattice parameters and the unit cell volume values are plotted in Fig. 6. The lattice shrinkage along the *c*-axis was estimated to be 0.4% over this temperature range, which was two times that along the *a*-axis (0.2%) because of the stacking structure of the  $\text{Ba}^{2+}$  and  $\text{NCN}^{2-}$  ions along the *c*-axis. The unit cell volume was reduced by 0.8% over this same temperature range, which would be associated with a reduction in the Ba–N bond length resulting in significant crystal field splitting of the 5d states. The reduced 5d energy position in turn decreases the energy difference between the ground  $4f^7$  state and the excited  $4f^65d^1$  state and induces a large red-shift in the emission wavelength.

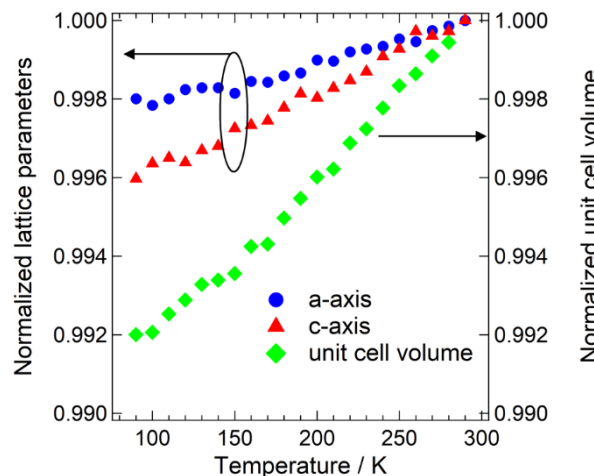


Figure 6 Temperature dependences of the normalized lattice parameters and unit cell volume. The lattice parameters (*a* and *c*) and unit cell volume have been normalized relative to the room temperature values (290 K).

No crystalline phase transition of the  $\text{BaCN}_2:\text{Eu}$  phosphor was observed in the powder XRD patterns between 138 K and 500 K as shown in Fig. S3. Tetragonal  $\text{BaCN}_2$  crystal structure was also confirmed at 90 K by using single crystal XRD (Tables S1 and S2). To further investigate the emission property depending on the temperature, fluorescence decay curves upon changing temperature were measured by monitoring 650 nm luminescence and shown in Fig. S4. The decay curves were fitted using a single exponential function to estimate the lifetime. Figure 7 shows the temperature dependence of lifetime for 5d level of  $\text{Eu}^{2+}$  doped in  $\text{BaCN}_2$  host lattice. From the lifetime, the quenching temperature,  $T_{1/2}$ , lifetime of 277 K was obtained and different from the  $T_{1/2}$  value estimated from the temperature dependence of emission intensity. It is already known that photoluminescence intensity as a function of temperature can be influenced by many factors such as the

changes in absorption strength with temperature and additional intensity by thermoluminescence.

Both radiative rate constant ( $k_r$ ) and nonradiative rate constant ( $k_{nr}$ ) were estimated by combination of the lifetime and estimated QE at different temperatures. Variation of  $k_r$  upon changing the temperature shown in Fig. S5 implies a change in crystal field splitting of the 5d states of  $\text{Eu}^{2+}$  with temperature<sup>42,43</sup>, which was induced by the significant change of the lattice parameters.

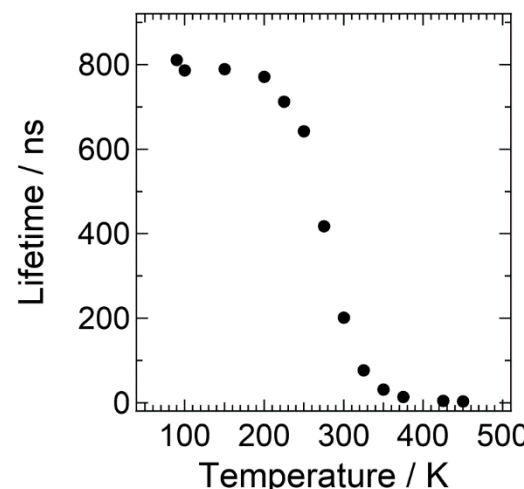


Figure 7 Temperature dependence of lifetime.

Interestingly, this wide variation in the emission spectrum upon changing the temperature could have applications in temperature sensing devices<sup>41</sup>. Optical temperature sensing has been previously investigated using various molecules and phosphors having multi emission-center<sup>44–46</sup>. The pronounced temperature dependence of the emission wavelength of the  $\text{BaCN}_2:\text{Eu}^{2+}$  phosphor is attributed to changes in the crystal field strength resulting from the varying distance between Eu and N atoms. The  $\text{BaCN}_2$  was also found to have large thermal expansion coefficients,  $\alpha_a = 1.5 \times 10^{-5} \text{ K}^{-1}$  and  $\alpha_c = 2.3 \times 10^{-5} \text{ K}^{-1}$  at 290 K, as estimated from the lattice parameters. These values are almost one order of magnitude larger than that of  $\text{Si}_3\text{N}_4$  ( $3.0 \times 10^{-6} \text{ K}^{-1}$ )<sup>47</sup>. The relatively “soft” host lattice of the  $\text{BaCN}_2$  thus leads to a wide variation in the emission wavelength with temperature, induced by changes in the crystal field splitting of the 5d energy levels of  $\text{Eu}^{2+}$  ions. The  $\text{BaCN}_2:\text{Eu}$  obtained in this work is highly air-sensitive. Recently, we found the product is stable in organic solvents such as hexane and acetone and silicone resin. Moisture resistive coating in organic solution should be further investigated to realize the applications in temperature sensing phosphor.

## Conclusion

A new form of  $\text{BaCN}_2$  with a tetragonal structure was prepared by a simple nitridation reaction of  $\text{BaCO}_3$  under an  $\text{NH}_3$  flow. The crystal structure is an isotype of that of alkaline cyanates ( $\text{AOCN}$ ,  $\text{A} = \text{K, Rb, Cs}$ ), in which  $\text{Ba}^{2+}$  ion is coordinated with

eight N atoms in  $[N=C=N]^{2-}$  groups to construct a regular square antiprism environment. Eu<sup>2+</sup>-doped tetragonal BaCN<sub>2</sub> exhibited a strong red emission peak at 660 nm in response to irradiation with blue or green light and showed relatively small thermal quenching compared with other cyanate and thiocyanate phosphors. The red emission shifts toward longer wavelengths (up to 680 nm) upon decreasing the measurement temperature, as a result of shrinkage of the host lattice. The present results demonstrated that Eu<sup>2+</sup>-doped BaCN<sub>2</sub> is a promising new red-emitting phosphor to be utilized in temperature sensing device.

## Conflicts of interest

There are no conflicts to declare.

## Acknowledgements

This work was partly supported by a JSPS Grants-in-Aid for Scientific Research on Innovative Areas "Mixed Anion" (grant numbers JP16H06439 and JP16H06441). This work was also performed under the Cooperative Research Program of "Network Joint Research Center for Materials and Devices."

## Notes and references

- 1 R. J. Xie and H. T. Hintzen, *J. Am. Ceram. Soc.*, 2013, **96**, 665.
- 2 L. Chen, C. C. Lin, C. W. Yeh, and R. S. Liu, *Mater.*, 2010, **3**, 2172.
- 3 Z. Xia, Z. Xu, M. Chen, and Q. Liu, *Dalton Trans.*, 2016, **45**, 11214.
- 4 R. J. Xie, and N. Hirosaki, *Sci. Technol. Adv. Mater.*, 2007, **8**, 588.
- 5 R. J. Xie, N. Hirosaki, K. Sakuma, and N. Kimura, *J. Phys. D: Appl. Phys.*, 2008, **41**, 144013.
- 6 M. Krott, X. Liu, B. P. T. Fokwa, M. Speldrich, H. Lueken, and R. Dronskowski, *Inorg. Chem.*, 2007, **46**, 2204.
- 7 K. Morita, G. Mera, K. Yoshida, Y. Ikuhara, A. Klein, H. J. Kleebe, and R. Riedel, *Solid State Sci.*, 2013, **23**, 50.
- 8 G. Baldinozzi, B. Malinowska, M. Rakib, and G. Durand, *J. Mater. Chem.*, 2002, **21**, 268.
- 9 X. Liu, M. Krott, P. Muller, C. Hu, H. Lueken, and R. Dronskows, *Inorg. Chem.*, 2005, **44**, 3001.
- 10 M. Krings, G. Montana, R. Dronskowski, and C. Wickleder, *Chem. Mater.*, 2011, **23**, 1694.
- 11 A. Cochet, *Angew. Chem.*, 1931, **44**, 367.
- 12 A. Perret, and A. M. Krawezynski, *Helv. Chim. Acta*, 1932, **15**, 1009.
- 13 S. Yuan, Y. Yang, F. Chevire, F. Tessier, X. Zhang, and G. Chen, *J. Am. Ceram. Soc.*, 2010, **93**, 3052.
- 14 U. Berger, and W. Schnick, *J. Alloys Compd.*, 1994, **206**, 179.
- 15 K. G. Strid, *Z. Anorg. Allg. Chem.*, 1968, **360**, 205.
- 16 S. Pagano, G. Montana, C. Wickleder, and W. Schnick, *Chem. Eur. J.*, 2009, **15**, 6186.
- 17 C. Wickleder, *Chem. Mater.*, 2005, **17**, 1228.
- 18 C. Wickleder, *J. Alloys Compd.*, 2004, **374**, 10.
- 19 B.A.I. APEX2, Madison, WI, USA, 2014.
- 20 B.A.I. SADABS v. 2014/5, Madison, WI, USA, 2015.
- 21 G. M. Sheldrick, *Acta Crystallogr. A*, 2015, **71**, 3.
- 22 K. Momma, and F. Izumi, *J. Appl. Crystallogr.*, 2011, **44**, 1272.
- 23 F. Izumi, and K. Momma, *Solid State Phenom.*, 2007, **130**, 15.
- 24 S. B. Hendricks, and L. Pauling, *J. Am. Chem. Soc.*, 1925, **47**, 2904.
- 25 T. C. Waddington, *J. Chem. Soc.*, 1959, **0**, 2499.
- 26 X. Liu, A. Decker, D. Schmitz, and R. Dronskowski, *Z. Anorg. Allg. Chem.*, 2000, **626**, 103.
- 27 A. Hosono, Y. Masubuchi, T. Endo, and S. Kikkawa, *Dalton Trans.*, 2017, **46**, 16837.
- 28 M. Krings, M. Wessel, W. Wilsmann, P. Muller, and R. Dronskowski, *Inorg. Chem.*, 2010, **49**, 2267.
- 29 L. G. van Uitert, *J. Lumin.*, 1984, **29**, 1.
- 30 R. J. Xie, N. Hirosaki, T. Takeda, and T. Suehiro, *ECS J. Solid State Sci. Technol.*, 2013, **2**, R3031.
- 31 Y. Q. Li, J. E. J. van Steen, J. H. W. van Krevel, G. Botty, A. C. A. Delsing, F. J. DiSalvo, G. de With, and H. T. Hintzen, *J. Alloys Compd.*, 2006, **417**, 273.
- 32 P. Pust, V. Weiler, C. Hecht, A. Tücks, A. S. Wochnik, A. K. Henb, D. Wiechert, C. Scheu, P. J. Schmidt, and W. Schnick, *Nat. Mater.*, 2014, **13**, 891.
- 33 K. Shioi, N. Hirosaki, R. J. Xie, T. Takeda, and Y. Q. Li, *J. Mater. Sci.*, 2010, **45**, 3198.
- 34 K. Uheda, N. Hirosaki, Y. Yamamoto, A. Naito, T. Nakajima, and H. Yamamoto, *Electrochem. Solid-State Lett.*, 2006, **9**, H22.
- 35 P. Dorenbos, *J. Phys.: Condens. Matter*, 2003, **15**, 575.
- 36 G. J. Dirksen and G. Blasse, *J. Solid State Chem.*, 1991, **92**, 591.
- 37 A. Diaz and D. A. Kesler, *Mater. Res. Bull.*, 1996, **31**, 147.
- 38 A. Meijerink and G. Blasse, *J. Lumin.*, 1989, **43**, 283.
- 39 H. Watanabe and N. Kijima, *J. Alloys Compd.*, 2009, **475**, 434.
- 40 Y. Q. Li, G. de With, and H. T. Hintzen, *J. Solid State Chem.*, 2008, **181**, 515.
- 41 X. D. Wang, O. S. Wolfbeis, and R. J. Meier, *Chem. Soc. Rev.*, 2013, **42**, 7834.
- 42 Y. Hasegawa, S. Tsuruoka, T. Yoshida, H. Kawai, and T. Kawai, *J. Phys. Chem. A*, 2008, **112**, 803.
- 43 T. Arakawa, M. Takakuwa, and J. Shiokawa, *Inorg. Chem.*, 1985, **24**, 3807.
- 44 P. Low, B. Kim, N. Takama, and C. Bergaud, *Small*, 2008, **4**, 908.
- 45 K. Miyata, Y. Konno, T. Nakanishi, A. Kobayashi, M. Kato, K. Fushimi, and Y. Hasegawa, *Angew. Chem. Int. Ed.*, 2013, **52**, 6413.
- 46 F. Venturini, R. Bürgi, S. M. Borisov, and I. Klimant, *Sens. Actuators A*, 2015, **223**, 324.
- 47 S. Iwai and A. Yasunaga, *Die Naturwissenschaften*, 1959, **46**, 473.